

**Thermal Performance of Laminate-to-Aluminum Attachment Materials and  
Non-Uniform Thermal Properties of an Alumina Granule/Epoxy Potting  
Compound**

by

John Franklin Maddox, Jr.

A thesis submitted to the Graduate Faculty of  
Auburn University  
in partial fulfillment of the  
requirements for the Degree of  
Master of Science

Auburn, Alabama  
May 10, 2010

Keywords: thermal conductivity, delamination, thermal adhesive, pressure sensitive adhesive, epoxy, alumina granules

Copyright 2010 by John Franklin Maddox, Jr.

Approved by:

Sushil H. Bhavnani, Co-Chair, Professor of Mechanical Engineering  
Roy W. Knight, Co-Chair, Professor of Mechanical Engineering  
Jeyhoon M. Khodadadi, Professor of Mechanical Engineering

## Abstract

A non-destructive method was used to determine the effects of thermal cycling on the thermal performance of a PCB attached to an aluminum substrate with a thermal adhesive. This method allows for a comparison of the thermal performance of various TIMs in an industrial application.

Testing was done on FR4 and Flex boards, both with and without overmolding, attached using PSA and an alternative adhesive. Baseline measurements were taken, then the boards were cycled from -40 to 125°C on a 90-minute cycle with 15-minute dwells at the target temperatures. It was found that both adhesives showed an increase in thermal conductivity, possibly due to curing, and delamination occurred at 17 out of 35 locations with the alternative adhesive within the first 1000 cycles while no delamination occurred with the PSA.

In harsh environments, including high shock and vibration, magnetic devices such as transformer coils are potted to enhance thermal performance and provide mechanical protection. One potting compound frequently used is epoxy containing alumina particles. A nominally isotropic and uniform potting compound consisting of about 70 to 80% by volume 14-28 mesh (0.6 to 1.2 mm across) alumina granules in low viscosity epoxy was tested to determine its thermal properties. Examination by optical microscopy revealed that there was significant variation in volume fraction of alumina particles by location. The specific heat and thermal conductivity of the compound were measured using a Differential Scanning Calorimeter and guarded heater method based on the ASTM D5470-06. The thermal properties were found to vary with time, location, and temperature; with the specific heat ranging from  $1.00 \text{ J/g}^\circ\text{C} \pm 14\%$  at  $25^\circ\text{C}$  to  $1.22 \text{ J/g}^\circ\text{C} \pm 12\%$  at  $125^\circ\text{C}$  and an apparent thermal conductivity of  $2.56 \text{ W/m} \cdot \text{K} \pm 23\%$ . Users of such compounds should be aware that the

thermal properties are not necessarily constant in time or uniform, and assuming that they are could lead to significant errors when modeling their performance.

In harsh environments, including high shock and vibration, magnetic devices such as transformer coils are potted to enhance thermal performance and provide mechanical protection. One potting compound frequently used is epoxy containing alumina particles. A nominally isotropic and uniform potting compound consisting of about 70 to 80% by volume 14-28 mesh (0.6 to 1.2 mm across) alumina granules in low viscosity epoxy was tested to determine its thermal properties. A large block, nominally 200 mm by 100 mm, of the potting compound was cast and samples were taken from various locations throughout: near the top, bottom, sides and middle. Examination by optical microscopy revealed that there was significant variation in volume fraction of alumina particles from sample to sample. Small alumina particles settled amongst the larger particles near the bottom of the cast block. Near the top of the cast block, only large particles were present, so the compound was proportionally more epoxy. The specific heat of the compound was measured using a Differential Scanning Calorimeter. It was noted that the specific heat of the samples changed significantly during testing. This was apparently due to the large block sample not having been completely cured before testing. After additional curing of the samples, the properties stopped changing. The specific heat was found to vary with location, with the value depending on the relative abundance of alumina granules. The thermal conductivity of samples from various regions was measured using a guarded heater method based on ASTM D5470-06. As with specific heat, the thermal conductivity was found to vary significantly with location, based on the relative abundance of alumina granules. Values are presented for the thermal properties and their relationship to alumina volume fraction is noted. Users of such compounds should be aware that the thermal properties are not necessarily constant in time or uniform, and assuming that they are could lead to significant errors when modeling their performance.

### Acknowledgments

The work was supported by the NSF Center for Advanced Vehicle and Extreme Environment Electronics (CAVE3).

## Table of Contents

Abstract . . . . .	ii
Acknowledgments . . . . .	iv
List of Illustrations . . . . .	vi
List of Tables . . . . .	viii
List of Abbreviations . . . . .	ix
1      Introduction . . . . .	1
2      Background . . . . .	2
3      Experimental Methodology . . . . .	6
3.1    Delamination . . . . .	6
3.2    Test Matrix . . . . .	9
3.3    Volume Fraction . . . . .	9
3.4    Specific Heat . . . . .	10
3.5    Thermal Conductivity . . . . .	13
4      Experimental Results . . . . .	18
4.1    Delamination . . . . .	18
4.2    Volume Fraction . . . . .	21
4.3    Specific Heat . . . . .	23
4.4    Thermal Conductivity . . . . .	24
5      Conclusion . . . . .	30
Bibliography . . . . .	32
Appendices . . . . .	35

## List of Illustrations

3.1	Fixture for measuring the junction resistance of a circuit board attached to an aluminum backing. . . . .	7
3.2	(a) Clamped configuration (b) Detail view of clamped configuration (c) Unclamped configuration (d) Detail view of unclamped configuration . . . . .	8
3.3	Typical thermal resistance data . . . . .	9
3.4	Schematic representation of an alumina/epoxy cast block and the location from which samples were taken to determine the properties of the material. .	10
3.5	Circuit layout for test vehicle . . . . .	11
3.6	Aluminum substrate attached to (a) Flex PCB, (b) FR4 PCB, and (c) FR4 PCB with overmolding. . . . .	12
3.7	Image used to determine the volume fraction of epoxy, where (a) is the original image and (b) is the image after the threshold tool has been used to distinguish between the epoxy region and the alumina region. . . . .	13
3.8	Guarded heater apparatus used to measure thermal conductivity. . . . .	14
3.9	Thermocouple reading are extrapolated to determine the temperature at the clamping surface and the heat flowing through the sample. . . . .	16
4.1	Thermal resistances of FR4 boards with PSA and an alternative adhesive prior to cycling . . . . .	19
4.2	Average junction resistance with cycling . . . . .	20
4.3	Average change in junction resistance with cycling . . . . .	21
4.4	Comparison of junction resistance for clamped and unclamped boards . . . .	22
4.5	Percent change in junction resistance of alternative adhesive boards without clamping . . . . .	23
4.6	Percentage of locations where delamination has occurred . . . . .	24

4.7	Cracking of overmolding A after 250 cycles . . . . .	25
4.8	Micrographs illustrating the variation in volume fraction of alumina by location, where (a) came from location C-3 and (b) came from location C-5. . . . .	26
4.9	Specific heat of a single sample measured four times with a DSC, twice in ramp mode and twice in scan mode. . . . .	26
4.10	Typical specific heat values for different locations. . . . .	27
4.11	Images of sample after performing a conductivity test, where (a) is the bottom, (b) is the side, and (c) is the top. (Note: the scale is in inches). . . . .	27
4.12	Changes in the material after being exposed exposed to 125°C for the given time, where at 3 days and 2 weeks the darker surfaces are the exterior color and the lighter surfaces are cross sections to show the interior color. . . . .	28
4.13	Micrographs showing the surface effects which occured after being held at 125°C for 2 weeks. . . . .	29

## List of Tables

3.1	Board configurations tested . . . . .	10
4.1	Volume fraction of alumina calculated using images taken from 20 locations.	22
4.2	Apparent thermal conductivity values measured at given temperatures. . . .	29

## List of Abbreviations

### Acronyms

DSC differential scanning calorimeter

RTD resistance temperature detector

TIM thermal interface material

### English letter symbols

$k_{mb}$  thermal conductivity of metering block, W/m · K

$L$  distance between metering blocks, m

$\dot{q}_s''$  heat flux, heat-transfer per unit area, at surface , W/m<sup>2</sup>

$R_{int}$  bulk thermal resistance between sample and metering block, W/m · K

### Greek letter symbols

$\Delta T$  temperature drop between metering blocks, K

$\lambda$  apparent thermal conductivity, W/m · K

### Subscripts

$bot$  bottom metering block

$top$  top metering block

## Chapter 1

### Introduction

Ceramic oxide filled polymers are being increasingly used in the area of electronics packaging. The motivation for this is that the composite retains the electrical and thermal properties of the ceramic while keeping the mechanical properties of the polymer. This allows the compound to be easily incorporated into the manufacturing process used to package electronics. One common polymer that is used is epoxy. Epoxy has the added benefit that by using different components and curing agents its final properties can be adjusted as desired.

A number of studies have looked at the effects of ceramic and metal powders in polymers. It has been shown that the mechanical properties [1, 2], electrical conductivity [3], dielectric constant [4], and thermal conductivity [2, ?] of metal and ceramic polymer composites show a beneficial increase with an increasing volume fraction of the embedded component. These attributes make it a good potting compound for harsh environment electronics.

Epoxy containing alumina granules is frequently used to encapsulate magnetic devices since it has a relatively high dielectric constant and thermal conductivity while still being conformal enough to be easily applied during assembly. The higher thermal conductivity of the potting compound helps to remove the heat generated by the device. The mechanical support supplied by the hardened resin helps to protect the device, especially in harsh environments with high shock and vibration.

## Chapter 2

### Background

The difference in coefficients of thermal expansion (CTE) between dissimilar materials causes shear stresses to be generated during normal operation of an electronic device. The cyclic nature of these stresses causes fatigue at the joints, which leads to cracking and ultimately failure. Minimizing the temperature change experienced by a device will diminish the effects of CTE stresses and thus lead to improved reliability. Therefore, the removal of heat has become an increasingly important aspect of electronics packaging in recent years.

The heat generated in an electronic device must eventually be rejected to the environment. This process is enhanced in a number of ways, usually with a heat sink of some kind being attached to the heat producing components in a device. However, the thermal resistance between the components and the heat sink can become a bottleneck if measures are not taken to decrease the contact resistance between the two. While the contact resistance could be decreased by pressing one surface against the other with sufficient force, this is not optimal from a reliability or manufacturing point of view. Another alternative is to use a thermal interface material (TIM). Some TIMs in use today are soft metals, thermal greases, epoxy resins, pressure sensitive adhesive tapes (PSA), phase change materials, and elastomer pads [5, 6]. The properties of these materials are often enhanced by the addition of judiciously selected particles to increase the bulk thermal conductivity of the material.

The use of a thermal adhesive as a TIM gives the added benefit of securing the two surfaces together without the need for external clamping. This reduces the complexity of a device by reducing the number of components and simplifies the manufacturing, as adhesives are relatively easy to apply when compared to the alternatives. Adhesives, both electrically

conductive and thermally conductive, are used in the assembly of many automotive electronics [7]. When used as a TIM in these applications, it is necessary that the adhesive exhibit reliable performance both mechanically and thermally. The effects of aging [8] and thermal cycling [9, 10, 11, 12, 13] on the mechanical strength of various adhesives have been well documented in the literature. However, there is less information about the effects of aging and thermal cycling on the thermal performance of these adhesives.

This paper will compare the thermal performance of two adhesives, PSA and a new alternative adhesive. PSA tapes are used in a variety of applications from everyday consumer products to, more recently, electronics assembly [14]. In the area of electronics assembly, PSA tapes have been developed for electrical insulation, electrical conduction, and thermal conduction [15, 16]. Of interest, in this paper, are the thermally conductive PSAs and their use as a TIM for connecting a printed circuit board (PCB) to an aluminum plate. The modes of failure due to separation at a polymer-metal interface were reported by Yao, et. al. [17], to be either adhesive failure or cohesive failure. Adhesive failure is when the separation occurs at the interface between the adhesive and the metal, while cohesive failure is when the separation occurs within the adhesive layer. It was reported that the mode of failure would depend primarily on the surface roughness of the metal. The effects of creep on the mechanical strength of PSA for heat sink attachment under isothermal conditions were reported by Eveloy, et. al. [11]. This paper will look at the effects of thermal cycling on the thermal resistance of PSA attached to an aluminum substrate. The measurement method used in this paper will not distinguish between adhesive and cohesive failure, but rather the failure of the bond due to separation will be generically referred to as delamination. At the conclusion of the study, a destructive analysis of the boards will be performed to determine the location of the failure.

Similar work to that being presented in this paper has been done by Eyman, et. al. [12] and Khuu, et. al. [13]. Eyman, et. al. [12] tested the effects of thermal cycling on the reliability of various methods for attaching heat sinks to plastic ball grid arrays (PBGA),

with PSA and heat cured epoxy being among the methods tested. Electrical continuity was used as the criterion for failure. Khuu, et. al. [13] used the laser flash method to measure the thermal performance of various thermal interface materials, with epoxy and gap pads attached with PSA among the tested materials.

The selection of a TIM depends on many factors, which need to be analyzed differently for each specific application. Since the overall thermal resistance of a TIM includes the thermal resistance of the TIM itself as well as the interface resistances between the TIM and the surfaces it touches, the bulk thermal conductivity is insufficient to fully characterize a TIM. The inadequacies of ASTM standards for measuring the performance of TIMs, as detailed by Lasance [18], make design decisions based on vendor-supplied data difficult. The data supplied by vendors are usually obtained with a standard pressure of 3 MPa being applied to the sample, which is much higher than what the TIM will experience in a real world application. It has been shown that contact resistance is greatly affected by changes in pressure [6]. Therefore, data collected with an unrealistically high pressure being applied cannot be reliably used to make design decisions for applications where the TIM will have a much lower pressure applied.

As suggested by Lasance [18], one possible solution to this problem is to implement application-specific tests. By applying various TIMs to a standardized package, meaningful comparisons can be made between the products with confidence that the resulting data is indicative of real world performance.

This study was conducted using a standardized package consisting of either a Flame Retardent 4 (FR4) or polyimide (denoted as Flex) PCB attached to an aluminum substrate with a thermal adhesive. The PCBs were attached to the aluminum substrate by the vendor to control for possible inconsistencies in manufacturing procedure. The two adhesives tested were PSA and an alternative adhesive (denoted as ALT). The boards were rapidly aged by thermally cycling from -40 to 125°C. The composite thermal resistance of the PCB, TIM,

and aluminum substrate was checked every 250 cycles using a procedure similar to the one presented by Knight, et. al. [19].

This study will also look at the effects of overmolding on the thermal performance of PSA. The overmoldings used are polyimide based and encapsulate the entire PCB and most of the aluminum substrate. Since it wraps around the PCB and substrate, the overmolding has the effect of mechanically holding the PCB in place. This will help to minimize the effects of delamination, however there is a trade off, as it inhibits the transfer of heat from the board. Two overmoldings were tested and they will be denoted as overmolding A and overmolding B.

While this study only measures the effects of thermal cycling on the thermal performance of the TIMs, related studies using the same standardized package have characterized the effects of thermal cycling on the reliability of the packages used to populate the board with PSA as the TIM [20, 21].

An epoxy, Stycast W-19, impregnated with tabular alumina, T64, is used as a potting compound for a power transformer. The alumina granules are packed around the device to be potted and the structure is subjected to sonic vibrations as the epoxy resin is allowed to fill in the empty spaces around the alumina. The vibration and the incorporation of a range of particle sizes result in an alumina volume fraction of approximately 70-80%, as will be reported later. This is higher than the expected maximum packing density for spherical particles of 64% [22], it is this high volume fraction of alumina that makes this composite useful as a potting compound.

In order to model and predict the performance of the system, it is necessary to have accurate values for the properties of the material. It is difficult to accurately predict the volume fraction, or packing density, of the alumina as well as the thermal properties. Therefore, the properties of the material will be determined experimentally so that it can be properly modeled.

## Chapter 3

### Experimental Methodology

#### **3.1 Delamination**

A fixture was constructed to measure the temperature at the top and bottom of a package while a fixed amount of heat is generated on the top of the PCB. A composite thermal resistance can be calculated from the temperature drop across the PCB, TIM, and aluminum substrate.

$$R_{jx} = \frac{T_j - T_x}{P} = \frac{\Delta T_{jx}}{P} \quad (3.1)$$

The resulting junction resistance can then be used to determine whether the PCB has delaminated from the aluminum substrate.

An operational schematic of the fixture used is shown in Figure 3.1. The aluminum substrate sits on top of a rubber gasket. The top of the fixture can be used to secure the sample in two ways. In the clamped configuration, the top of the fixture presses the PCB against the aluminum substrate, which is pressed against the bottom rubber gasket; this configuration is shown in Figure 3.2 parts (a) and (b). In the unclamped configuration, the top of the fixture presses against only the aluminum substrate and the PCB is allowed to remain free, this configuration is shown in Figure 3.2 parts (c) and (d). In each method, the top of the fixture is secured to the bottom of the fixture by four screws, each tightened to 25 ft-lbs. of torque.

Once the package has been mounted in the fixture, ethylene glycol is impinged on the back of the aluminum substrate. The temperature of the ethylene glycol is maintained at approximately 22°C by an automated chiller. A thermocouple is used to monitor the temperature of the fluid,  $T_x$ , and a thermistor, mounted on the PCB, is used to measure the

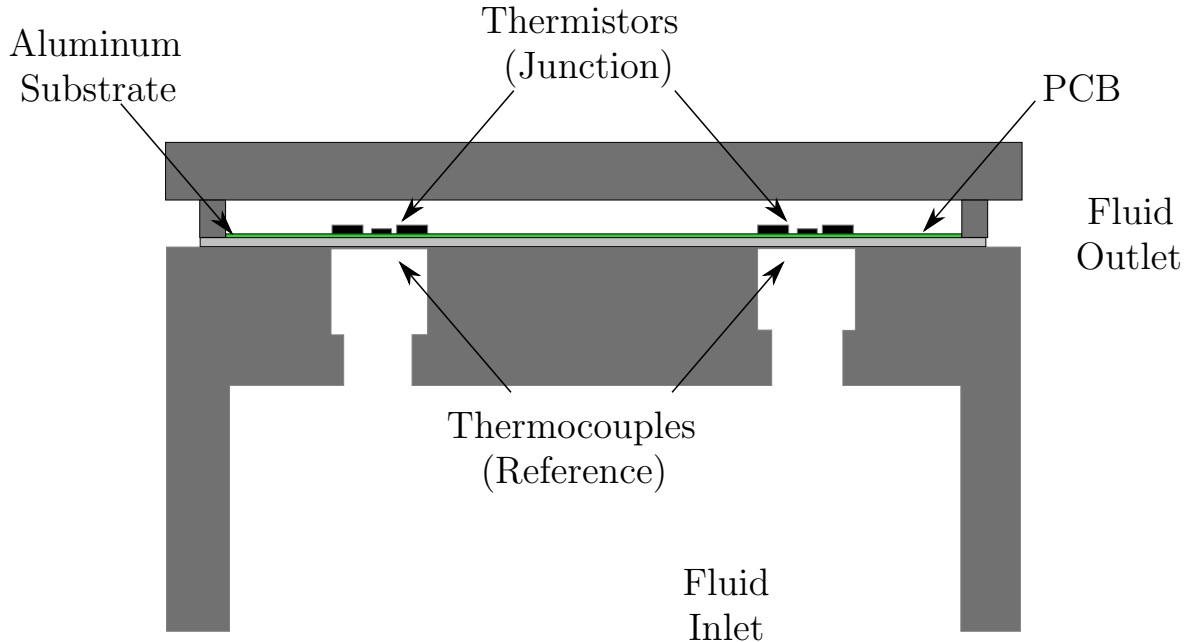


**Figure 3.1:** Fixture for measuring the junction resistance of a circuit board attached to an aluminum backing.

temperature at the top of the board,  $T_j$ . Four resistance heaters are used to generate a fixed amount of heat on the top surface of the board. The fixture is then sufficiently insulated so as to force heat from the resistors to move through the board and into the fluid on the backside of the metal plate.

Temperature readings were taken once the system reached steady state while generating 0, 0.5, 1.0, 1.5, and 2.0 Watts with the resistance heaters. Steady state was determined to have occurred when the temperature changed less than  $0.01^\circ\text{C}$  for 25 readings, or approximately five minutes. The temperature difference between the thermistor on the circuit board and the thermocouple in the fluid was then used to determine the junction resistance using a linear regression fit to the power data with an uncertainty of  $0.25^\circ\text{C}/\text{W}$ . A sample set of measurements for is shown in Figure 3.3.

The junction resistance is primarily a function of the thermal conductivities of the PCB, adhesive, and substrate and the contact areas of the PCB/adhesive and adhesive/substrate interfaces. Thermal cycling causes a decrease in the contact area, due to delamination, which increases the junction resistance. It also causes an increase in thermal conductivity, due to

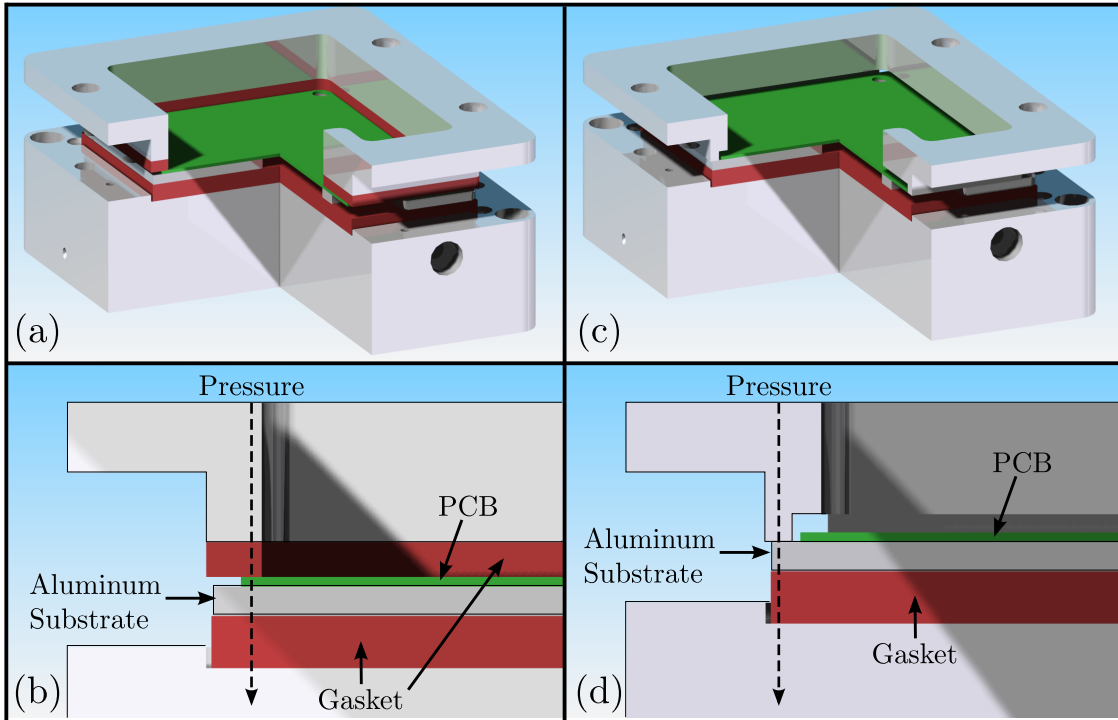


**Figure 3.2:** (a) Clamped configuration (b) Detail view of clamped configuration (c) Unclamped configuration (d) Detail view of unclamped configuration

curing, which decreases the junction resistance. In order to isolate the influence of these competing effects, the boards were tested in both the clamped and unclamped configurations. The measurements obtained, with the boards unclamped, include the effects of both the delamination and the change in thermal conductivity. However, the measurements obtained, with the boards clamped, primarily show the effects of the change in thermal conductivity of the adhesive. Therefore, the degree of delamination that has occurred can be determined by comparing the junction resistance of the unclamped boards to those of the clamped boards.

A large roughly cylindrical block, nominally 200 mm in diameter and 100 mm in height, of the potting compound was cast by the vendor to be representative of the final product as it would appear in a packaged device. Samples were taken from various locations throughout: near the top, bottom, sides and middle, as illustrated in Figure 3.4. The sectioning was done using a high-speed rotary diamond saw.

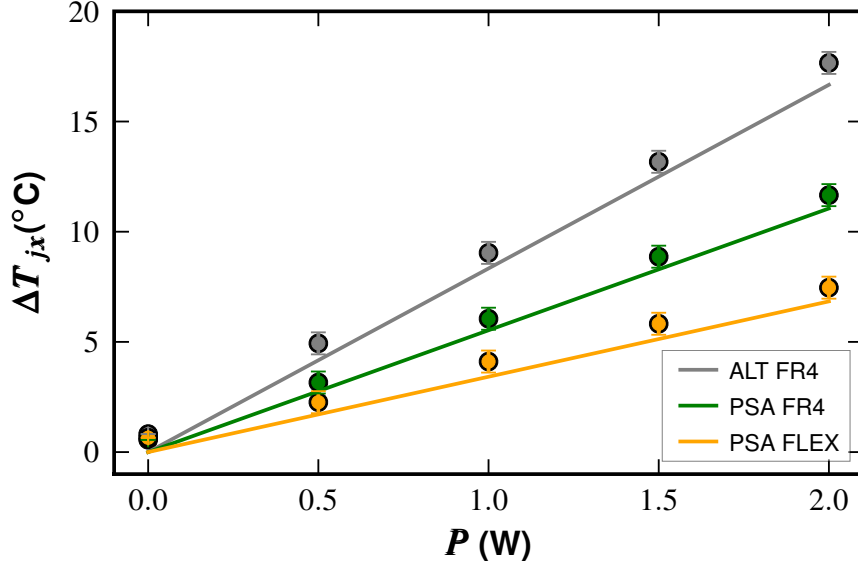


**Figure 3.3:** Typical thermal resistance data

### 3.2 Test Matrix

This study was conducted on 5 different configurations of board, adhesive, and overmolding. Each board had the standardized layout shown in Figure 3.5, with two test locations per board. Each test location consisted of a thermistor with four resistance heaters. The resistance heaters were arranged in a square to simulate the presence of a heat producing integrated circuit. The configurations tested are listed in Table 3.1 and sample boards are shown in Figure 3.6. The PCBs were attached to the aluminum substrate by the vendors.

### 3.3 Volume Fraction

The volume fraction of epoxy present in the sample was determined through the use of optical microscopy and image processing. Micrographs were taken of locations near the top, bottom, and middle of the block.

The images were processed by using a threshold tool to convert the color image to a black and white image with the epoxy regions being black and the alumina regions being white, as shown in Figure 3.7. The white pixels were counted and compared to the total number of pixels in the image to determine the percentage of the image occupied by the

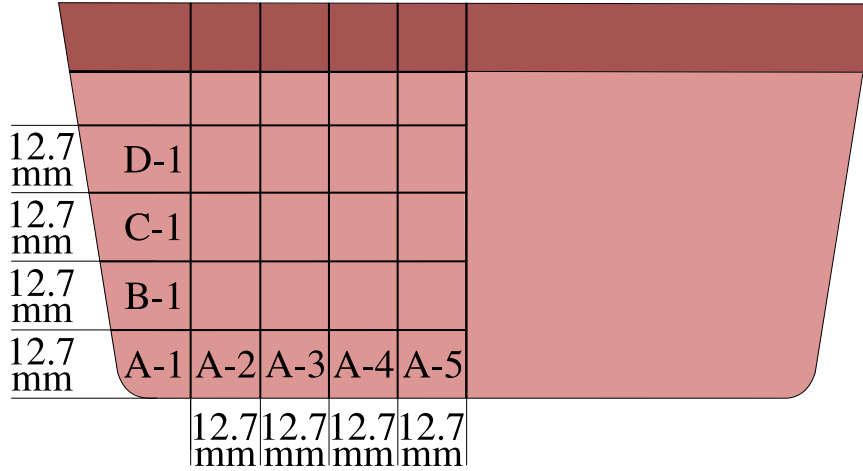


**Figure 3.4:** Schematic representation of an alumina/epoxy cast block and the location from which samples were taken to determine the properties of the material.

**Table 3.1:** Board configurations tested

# of Boards	PCB	Adhesive	Overmolding
10	Flex	PSA	
9	FR4	PSA	
17	FR4	ALT	
4	FR4	PSA	A
5	FR4	PSA	B

alumina.

$$\text{Volume Fraction}_{\text{alumina}} = \frac{\text{Pixels}_{\text{alumina}}}{\text{Pixels}_{\text{total}}} \quad (3.2)$$

This was repeated for multiple samples and an average was taken to find the volume fraction of the epoxy.

### 3.4 Specific Heat

The specific heat was measured using a Digital Scanning Calorimeter (DSC). A DSC works by keeping the sample being measured at approximately the same temperature as a known reference material. The difference in the amount of heat needed to maintain the sample and the reference material at the same temperature is used in conjunction with the

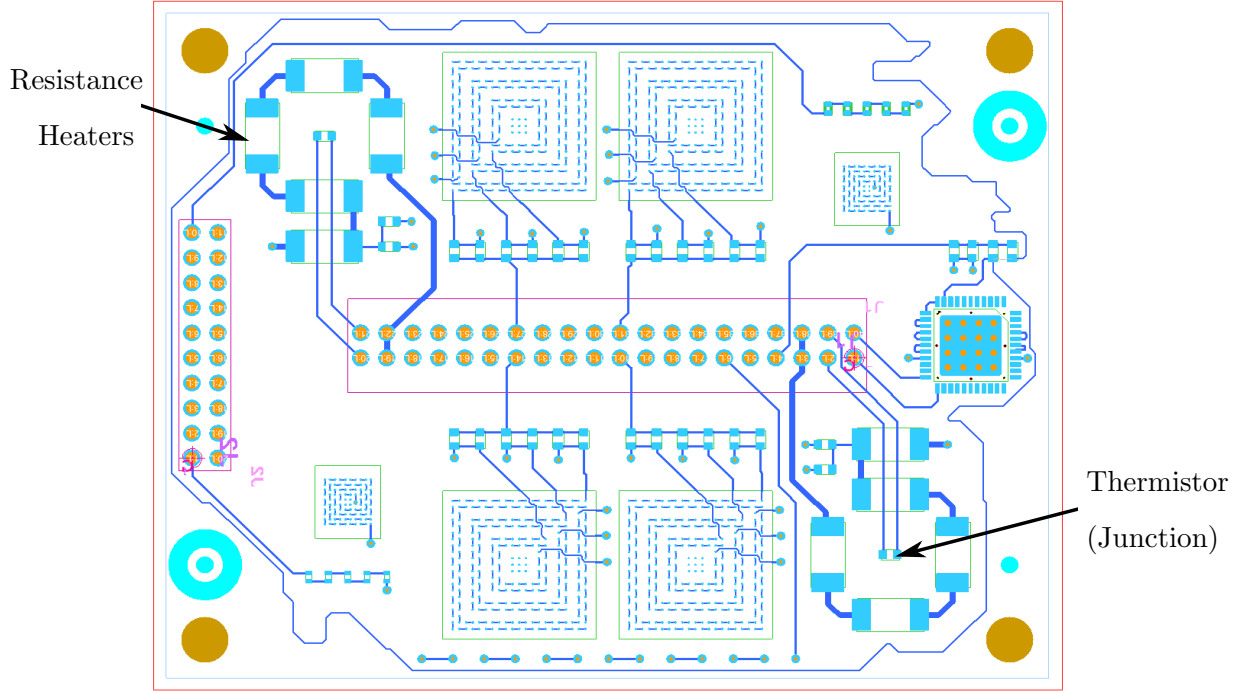
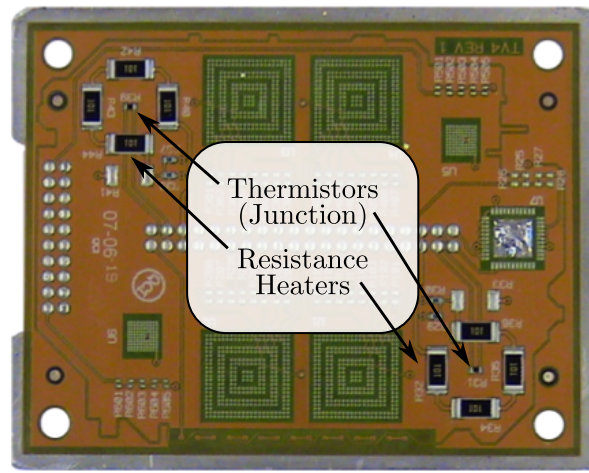


**Figure 3.5:** Circuit layout for test vehicle

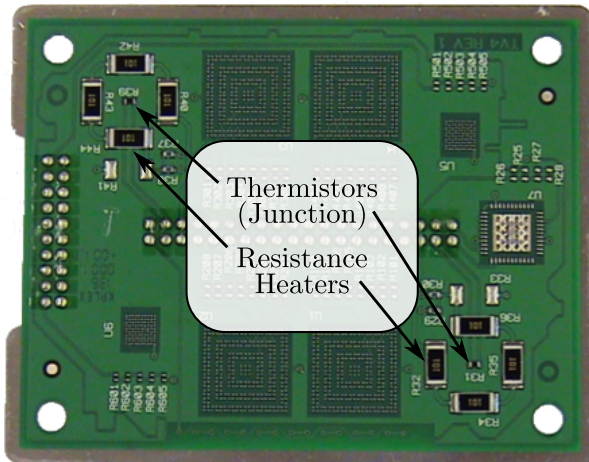
known properties of the reference material to calculate the specific heat of the sample being measured.

The DSC can be used in two modes, ramp mode and scanning mode. In ramp mode, a constant amount of heat is applied to both the sample and the reference material so that the temperature rise of the reference material is approximately linear. The sample and the reference material are brought from room temperature to the target high end temperature and then cooled to the target low end temperature. During this process, the temperature of the sample is recorded and combined with the known amount of heat being applied to the sample to generate a curve of the specific heat over the given temperature range.

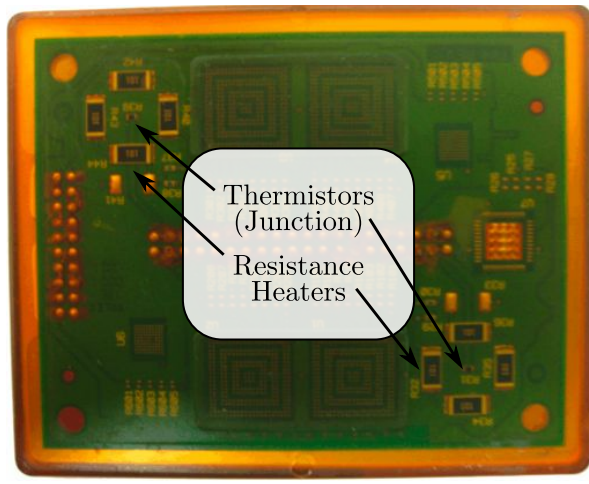
In scanning mode, the sample and the reference material are first brought to a target temperature. The sample and reference material are then repeatedly heated and cooled so that their temperatures oscillate around the target temperature. The difference in heat required to keep the sample and the reference material at the same temperature is recorded and used to calculate the specific heat of the sample at the target temperature. This process



(a)



(b)



(c)

**Figure 3.6:** Aluminum substrate attached to (a) Flex PCB, (b) FR4 PCB, and (c) FR4 PCB with overmolding.

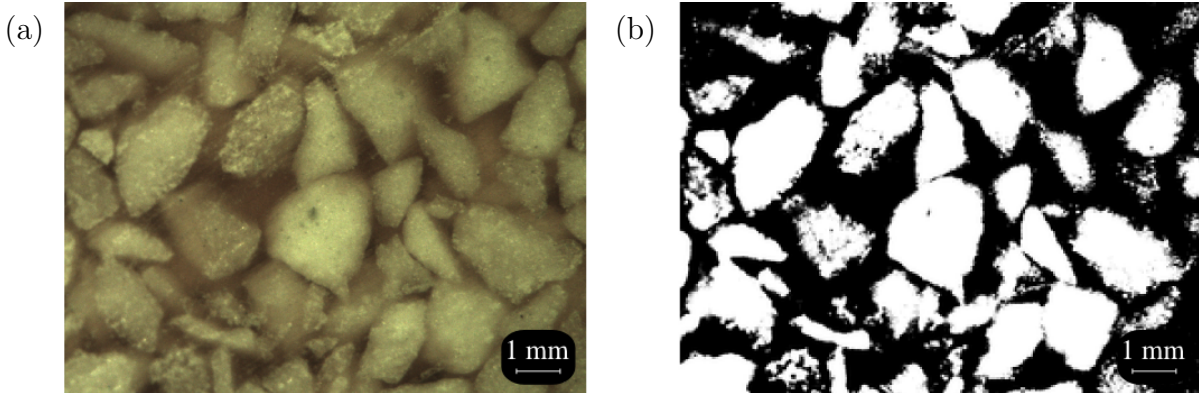


**Figure 3.7:** Image used to determine the volume fraction of epoxy, where (a) is the original image and (b) is the image after the threshold tool has been used to distinguish between the epoxy region and the alumina region.

is repeated at multiple temperatures to find points that can be used to generate a curve. While scanning mode has the advantage of being more accurate at a given temperature, it has the disadvantage of not being a continuous measurement for all temperatures within a given temperature range.

### 3.5 Thermal Conductivity

The thermal conductivity was measured using a guarded heater method based on the ASTM D5470-06 [23]. The apparatus, shown in Figure 3, consists of two metering blocks, each with five thermocouples spaced 1 cm apart. The sample being measured is placed between the two metering blocks. A temperature gradient is imposed across the metering blocks and the sample. The temperature readings from the thermocouples are used to determine the heat flow through and the temperature drop across the sample. An apparent thermal conductivity can then be calculated for the sample material.

The metering blocks were constructed from aluminum alloy 2024-T3. There are four resistance heaters, two rows of two, embedded below the thermocouples in the bottom metering block. A liquid cooled heat sink is mounted above the top metering block.

The thermal conductivity of the metering blocks,  $k_{mb}$ , was determined by using two DC power supplies to power the heaters. The upper row of heaters heated the metering

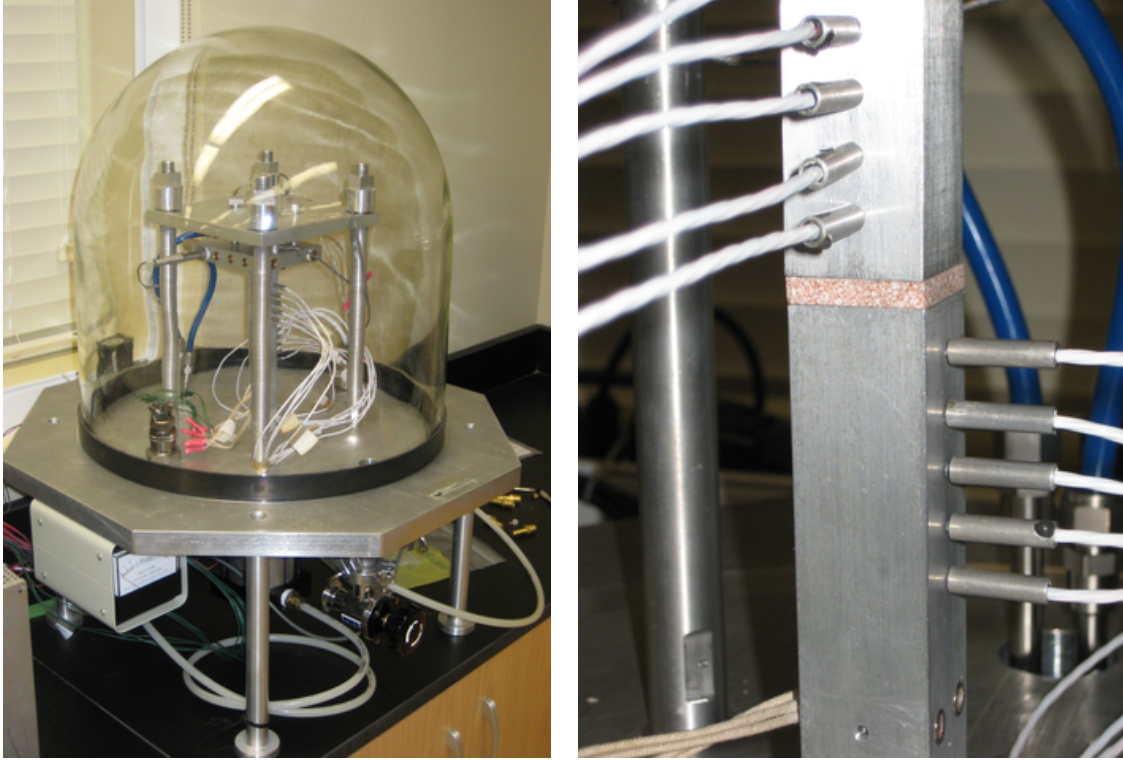


**Figure 3.8:** Guarded heater apparatus used to measure thermal conductivity.

blocks while the lower row acted as guard heaters. The temperature of each row of heaters was monitored by a Resistance Temperature Detector (RTD) embedded between the heaters. The power levels were then adjusted so that there was no temperature difference between the two rows of heaters. The heat flowing through the metering blocks was calculated from the electrical power generated by the top row of heaters. A least squares fit of the temperatures in the metering block was used to determine the thermal conductivity of the metering block material to be  $k_{mb} = 133 \text{ W/m} \cdot \text{K}$ . Further details of the calibration process can be found in Elkady [24].

A pneumatic piston is used to apply a constant force of 1925 N (435 lbs.), to the sample during the test, which corresponds to a pressure of 3 MPa (435 psi). This is necessary because it will be assumed that the thermal interface resistance between the sample and the metering blocks will be constant between tests.

A thermal interface material (TIM) is placed between the sample and each of the clamping surfaces. This helps to minimize the interface resistance between the sample and the metering block, but more importantly it helps to keep the interface resistance constant between samples. The TIM chosen was Sil-Pad® 800 with a thickness of 5 mil (0.127 mm) and a manufacturer reported thermal conductivity of 1.6 W/m · K. The contact resistances on either side of the TIM and the conductive resistance of the TIM will be combined into a single term,  $R_{int}$ , and will be assumed to be constant. The heat, generated below the bottom metering block, is removed by a serpentine liquid cooled heat sink mounted above the top metering block. The temperature of the inlet water to the heat sink is controlled by an external chiller.

The amount of heat flowing through the metering blocks is controlled by adjusting the power supplied to the heaters, which in turn controls the temperature drop across the sample. The temperature of the top metering block is controlled by adjusting the temperature of the inlet water to the heat sink, which in turn controls the mean temperature of the sample. By adjusting the power supplied to the heaters and the temperature of the water supplied to the heat sink, the apparatus can be used to measure the apparent thermal conductivity of a material over a range of temperatures.

To test a sample, it is clamped between the metering blocks, with a layer of TIM on each side. The heaters are powered and the temperature of the inlet water is adjusted so the mean temperature of the sample is at the desired temperature. The system is assumed to be at steady state when the temperature readings have been stable for at least 60 minutes.

A least squares fit of the thermocouple readings is extrapolated to find the temperature at each of the clamping surfaces, as illustrated in Figure 3.9. The slope of the least squares fit is also used, in conjunction with the known thermal conductivity of the metering blocks,

to find the heat flux through each of the metering blocks.

$$\dot{q}_{bot}'' = -k_{mb} \frac{\partial T}{\partial x} \Big|_{bot} \quad (3.3)$$

$$\dot{q}_{top}'' = -k_{mb} \frac{\partial T}{\partial x} \Big|_{top} \quad (3.4)$$

The average of the heat flux through the metering blocks is taken to be the heat flux through the sample.

$$\dot{q}'' = \frac{\dot{q}_{bot}'' + \dot{q}_{top}''}{2} \quad (3.5)$$

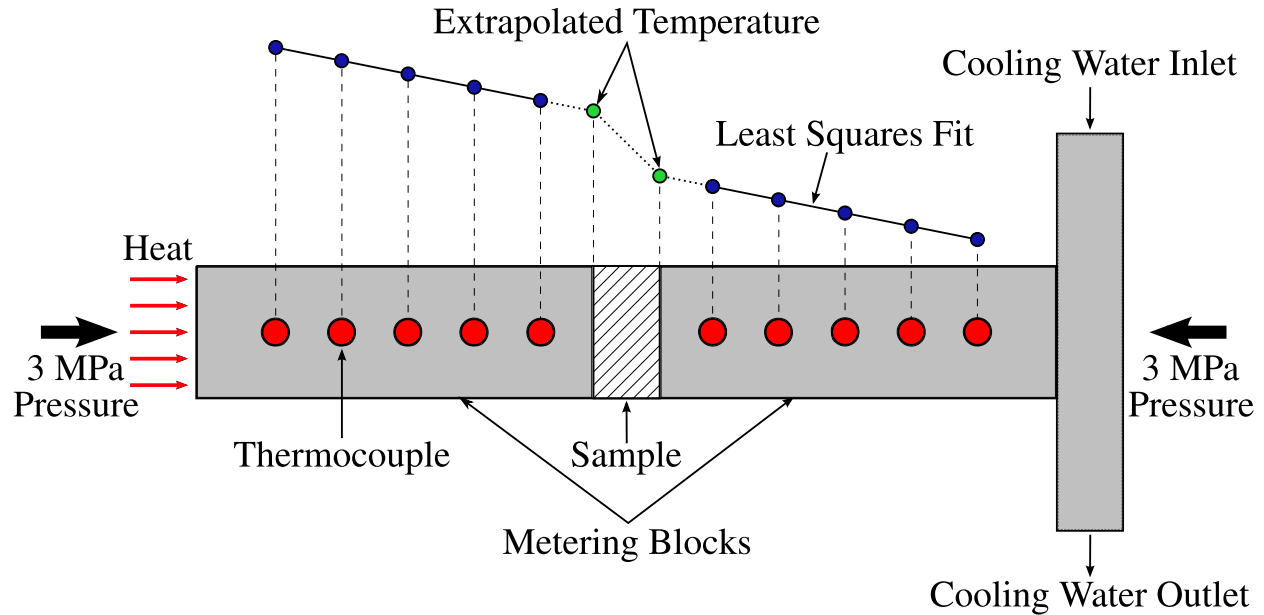


**Figure 3.9:** Thermocouple reading are extrapolated to determine the temperature at the clamping surface and the heat flowing through the sample.

Multiple samples of varying thicknesses are tested, and it is assumed that  $\lambda$  and  $R_{int}$  are constant between tests. The apparent thermal conductivity can then be obtained from

the least squares solution to the following equation:

$$\begin{bmatrix} 2 & L_1 \\ \vdots & \vdots \\ 2 & L_i \end{bmatrix} \cdot \begin{bmatrix} R_{int} \\ L_i \end{bmatrix} = \begin{bmatrix} \Delta T_1 / \dot{q}_1'' \\ \vdots \\ \Delta T_i / \dot{q}_i'' \end{bmatrix} \quad (3.6)$$

## Chapter 4

### Experimental Results

#### 4.1 Delamination

Prior to cycling, measurements were taken for each board as a baseline. The baseline measurements for PSA and the alternative adhesive on FR4 boards are shown in Figure 4.1, where it can be seen that the alternative adhesive exhibited a larger range of thermal resistances than did the PSA. The alternative adhesive boards ranged from 4.65 to 8.33°C/W with a standard deviation of 0.95°C/W, while the PSA boards ranged from 5.23 to 6.35°C/W with a standard deviation of 0.26°C/W. This suggests a non-uniform application of the alternative adhesive during manufacture.

The thermal resistance of the boards while clamped is shown in Figure 4.2, where it can be seen that the Flex boards had a lower junction resistance than the FR4 boards. This difference in performance is mainly due to the smaller contribution of the Flex PCB to the junction resistance since the Flex is thinner than the FR4. The configurations with the FR4 boards all had comparable performance, with the PSA boards having a slightly lower average thermal resistance than the alternative adhesive boards.

Figure 4.3 shows the change in the junction resistance of the boards while clamped. In each configuration, the thermal performance improved with thermal cycling, with the exceptions to this trend falling within the measured uncertainty. This is possibly due to curing of the adhesive, which increases its thermal conductivity. Since the PCBs were being pressed against the aluminum substrate, the changes observed are primarily due to changes in material properties, namely thermal conductivity. Similar initial improvements in thermal performance were reported by Khuu, et. al. [13].

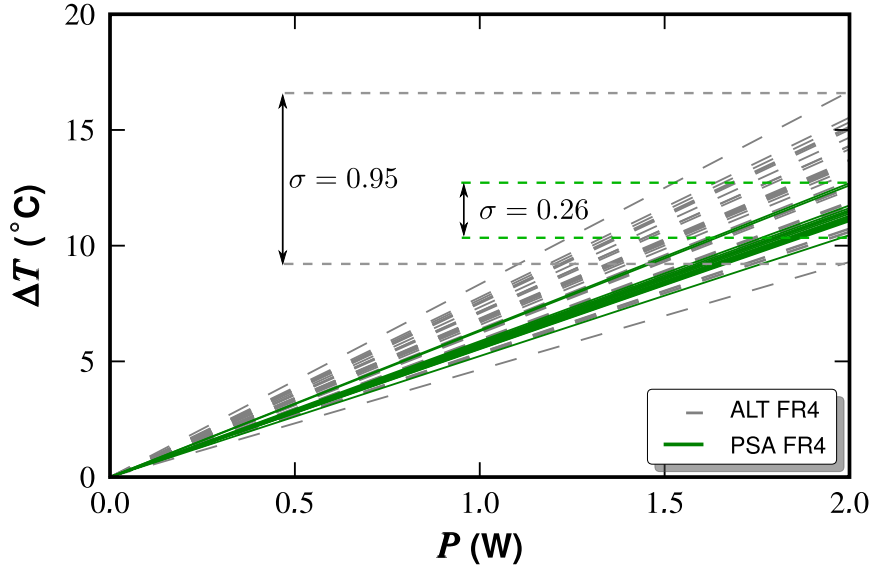


**Figure 4.1:** Thermal resistances of FR4 boards with PSA and an alternative adhesive prior to cycling

The delamination of the PCB from the aluminum substrate causes a significant increase in the contact resistance between the board and the substrate. Measuring the junction resistance while not pressing on the board allows for the detection of delamination. It was found that there was no significant difference between the clamped and unclamped readings for the PSA boards after 1000 cycles, therefore it was determined that no delamination had occurred. However, there were significant differences between the clamped and unclamped readings for the alternative adhesive boards.

While there was visible separation of the board from the aluminum substrate in some of the alternative adhesive boards, the only indication of delamination in others was the increase in the junction resistance. The boards were separated into three categories: no delamination, partial delamination, and full delamination. A board was considered to have partial delamination if the unclamped junction resistance was 25% greater than the clamped junction resistance or full delamination if it was 50% greater. Typical results for the alternative adhesive boards showing no delamination, partial delamination, and full delamination are shown in Figure 4.4, and the percent difference between the clamped and unclamped configurations for each of the alternative adhesive boards is shown in Figure 4.5. Using this

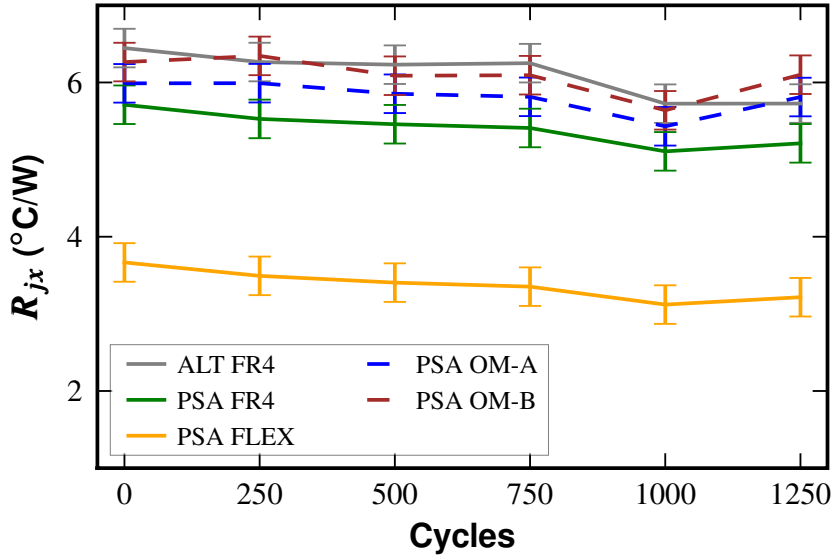


**Figure 4.2:** Average junction resistance with cycling

criterion resulted in partial delamination being present at five locations and full delamination at 12 locations in the alternative adhesive boards after 1000 cycles, while there was no delamination present in the PSA boards, as shown in Figure 4.6. This supports the findings of Eyman, et. al. [12], who reported no failures in PSA attached heat sinks until around 8,000 cycles, where as a heat cured epoxy started failing at around 300 cycles.

The overmolded boards showed an improvement in performance, while clamped, similar to the non-overmolded boards. There was an initial increase in the junction resistance for both types of overmolding, however this increase was within the measured uncertainty.

The overmolded boards did not show signs of delamination. However, due to the way they are constructed, it is not possible to hold them in the fixture without applying downward pressure on the circuit board. Because of this, the presence of delamination cannot be conclusively determined using the current method. It was seen that overmolding A exhibited cracks after 250 cycles as shown in Figure 4.7, while overmolding B showed no cracks after 1000 cycles.

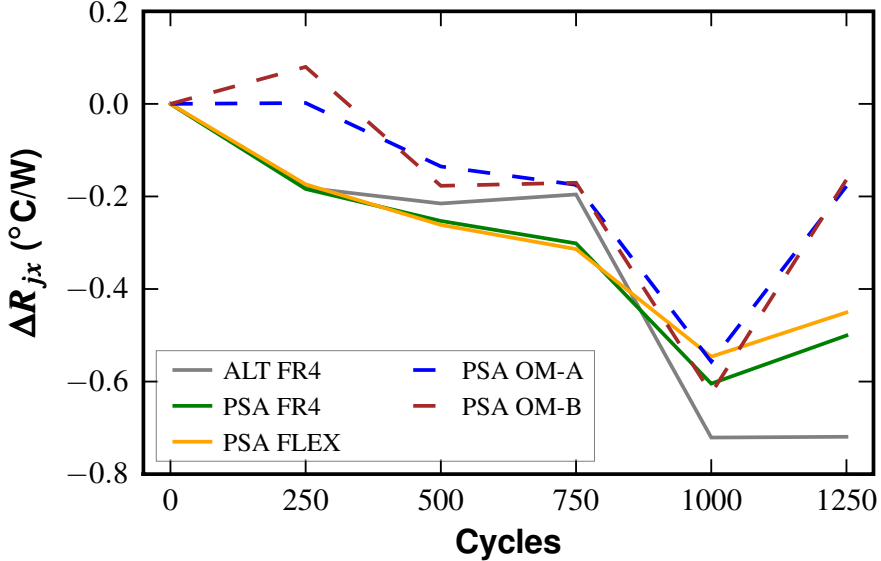


**Figure 4.3:** Average change in junction resistance with cycling

## 4.2 Volume Fraction

The volume fraction of the alumina was determined by taking the average of 20 samples. The samples were taken from four stratified layers, with five samples per layer, as shown in Figure 3.4.

Since the particles of alumina were heterogeneous in both size and shape, there was significant variation in the volume fraction by location. This variation occurred in both the axial and radial directions. Small alumina particles settled amongst the larger particles near the bottom of the cast block. Near the top of the cast block, only large particles were present, so the compound was proportionally more epoxy. Due to this, the volume fraction tended to decrease with increasing axial height. However, there was also some radial variation, i.e. two locations at the same stratum had different volume fractions of alumina, as illustrated in Figure 4.8. Therefore, in general, the volume fraction varied unpredictably by location. The results of combining the measurements from the 20 locations are summarized in Table 4.1.

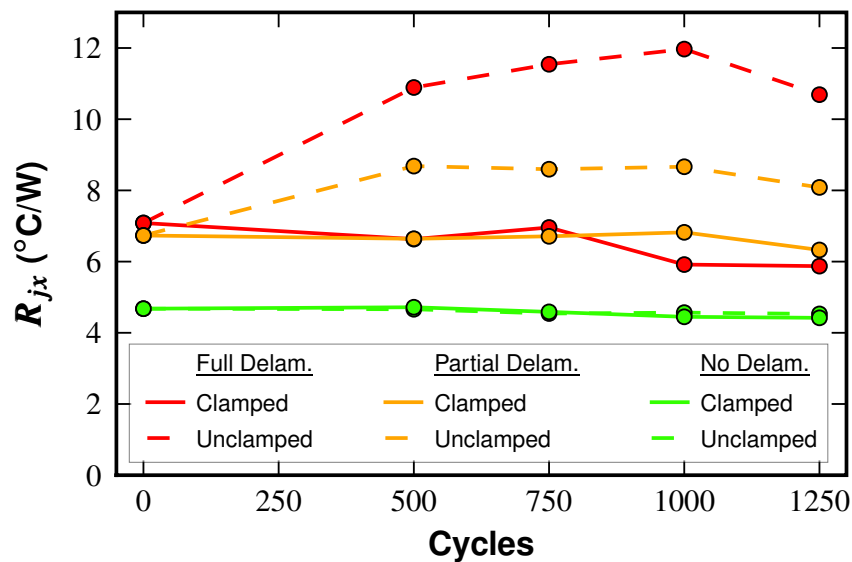


**Figure 4.4:** Comparison of junction resistance for clamped and unclamped boards

**Table 4.1:** Volume fraction of alumina calculated using images taken from 20 locations.

Volume Fraction of Alumina (%)	
Mean	74
$\sigma$	4
Maximum	69
Minimum	83

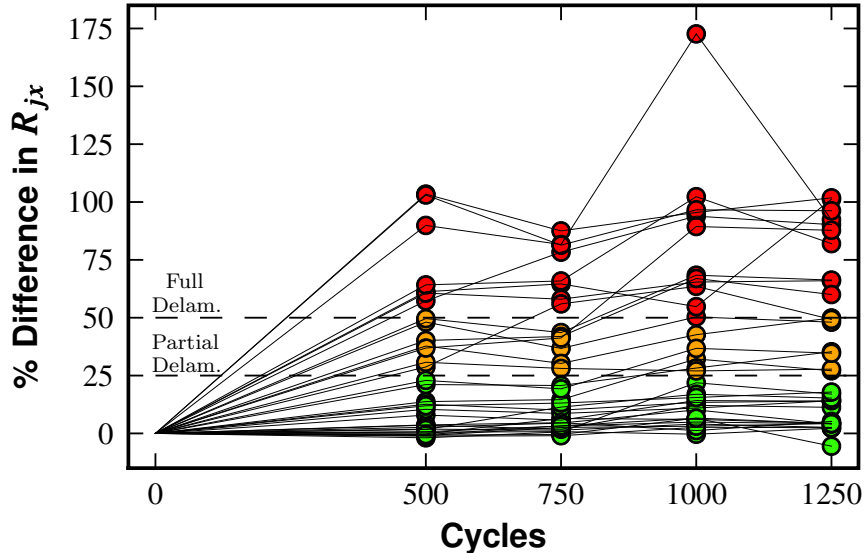


**Figure 4.5:** Percent change in junction resistance of alternative adhesive boards without clamping

### 4.3 Specific Heat

The specific heat of the material was found by measuring 20 samples, five radially spaced samples from four axial locations. Each sample was cut into the shape of a disc with a thickness of 1 mm and a diameter of 5 mm.

The samples were first tested in ramp mode and then in scanning mode. The results of the scanning mode test showed a significant departure from the results of the ramp mode test. In the first ramp mode test, as shown by the red line in Figure 4.9, the specific heat increases between 20 and 60°C, decreases drastically between 60 and 80°C, and then increases again between 80 and 135°C. However, as shown by the red dots in Figure 4.9, the first scanning mode test shows a steady increase in thermal conductivity with temperature over the entire temperature range. The trend seen in the scanning mode test is more representative of what was expected for this material. Because of this discrepancy, the samples were tested in both modes a second time, shown in blue in Figure 4.9. The second set of tests showed consistent readings for both modes. This suggests there was a residual chemical reaction

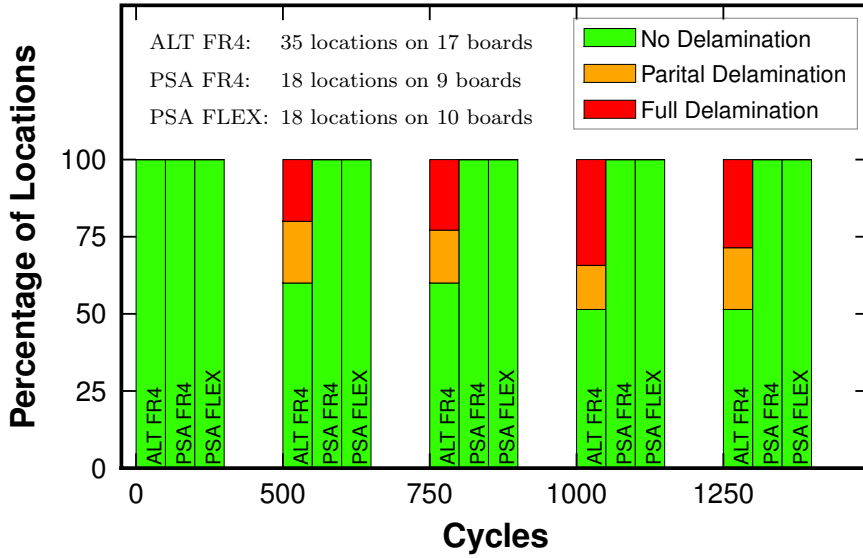


**Figure 4.6:** Percentage of locations where delamination has occurred

which occurred when the sample was heated during the first tests and that the reaction had completed by the time the second tests were run.

The specific heat was found to vary unpredictably with both axial and radial location. For example, as seen in Figure 4.10, at a given axial height, the sample taken from a outer radial location, C-2, and an inner radial location, C-5, yielded values that were lower than that of an intermediate sample, C-4. The values for the specific heat ranged from 0.86-1.14 J/g · K at 25C and 1.07-1.37 J/g · K at 125C.

#### 4.4 Thermal Conductivity

The thermal conductivity was measured using three samples of varying thicknesses. However, after completing the measurements, it was observed that the samples being tested had changed color, which suggests that they continued to cure during the test. As seen in Figure 4.11, the bottom surface, which was in contact with the hot metering block, was much darker than the top surface, which was in contact with the cold metering block. This color change is better illustrated by Figure 4.11(b) where it can be seen that the color gradient follows the imposed temperature gradient of dark to light and hot to cold respectively.

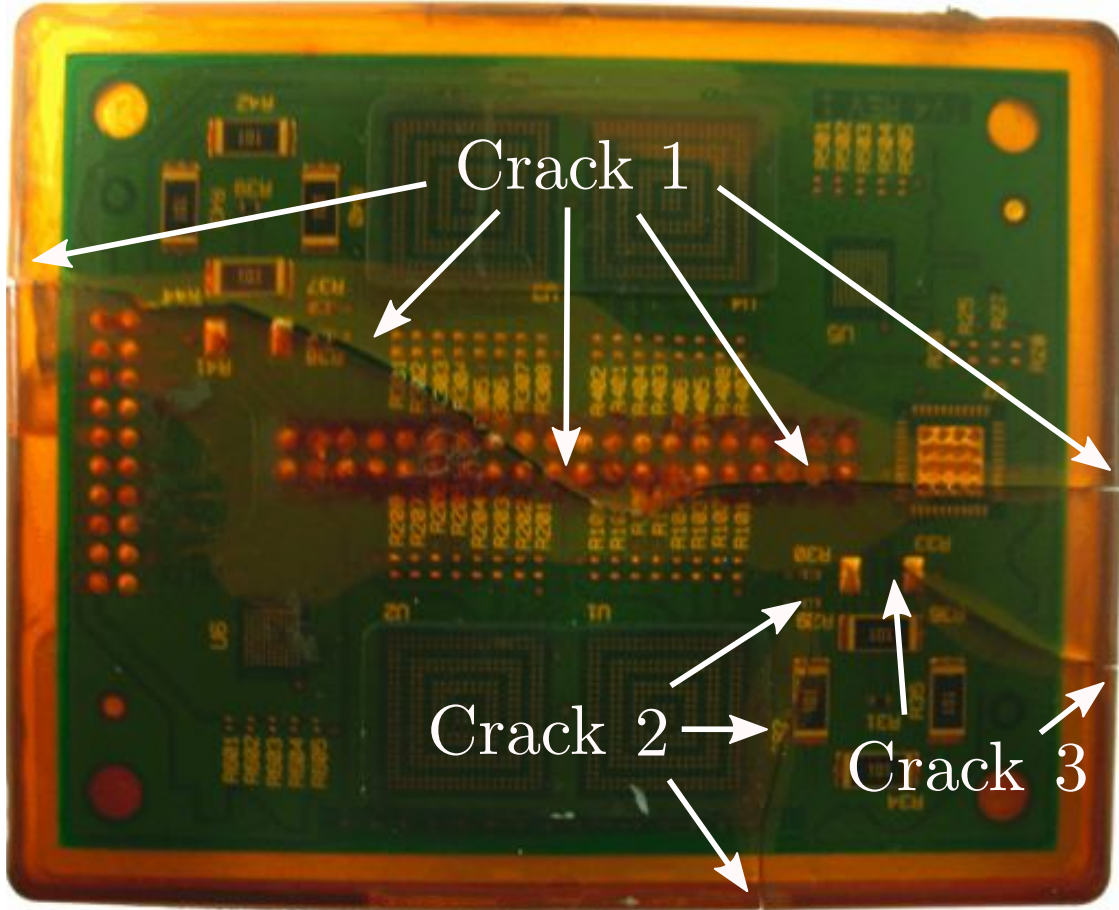


**Figure 4.7:** Cracking of overmolding A after 250 cycles

Although not shown in these images, the color of the material prior to the conductivity test was closer to that of Figure 4.11(c) than Figure 4.11(a).

The method used to determine the apparent thermal conductivity of the sample is dependent upon the system being at a steady state. Therefore, it is not possible to reliably determine the apparent conductivity of the material if the properties of the material are changing during the test, which in this case they appeared to be. Not only did the material appear to change during the test, but it also appeared to change non-uniformly, i.e. the top and bottom of the sample may not have the same properties since they appeared to have cured different amounts.

Since the discrepancies in the specific heat measurements appeared to be resolved by keeping the samples heated for an extended period of time, a similar process was taken

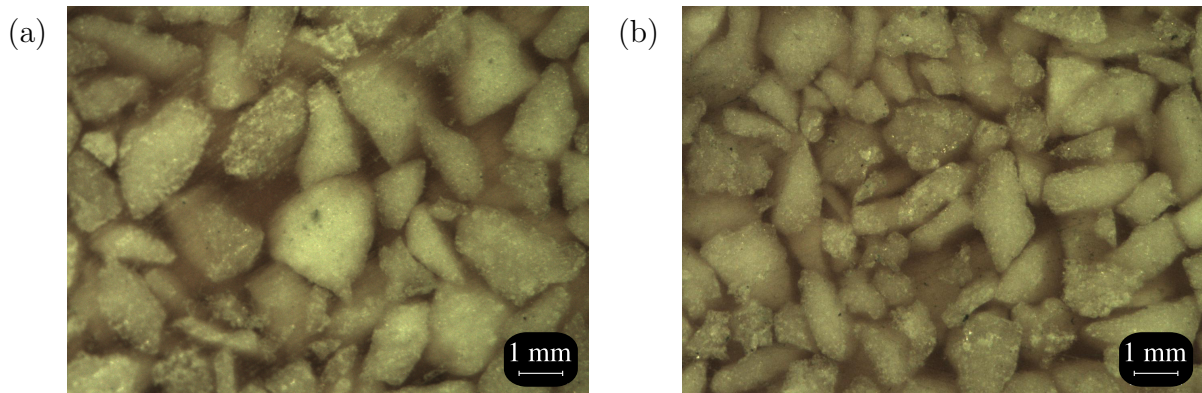


**Figure 4.8:** Micrographs illustrating the variation in volume fraction of alumina by location, where (a) came from location C-3 and (b) came from location C-5.

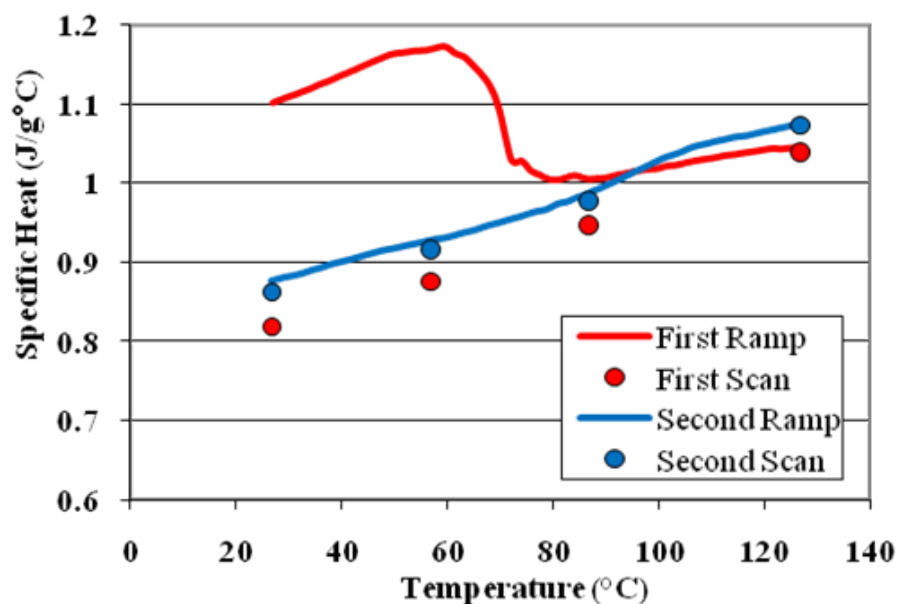


**Figure 4.9:** Specific heat of a single sample measured four times with a DSC, twice in ramp mode and twice in scan mode.

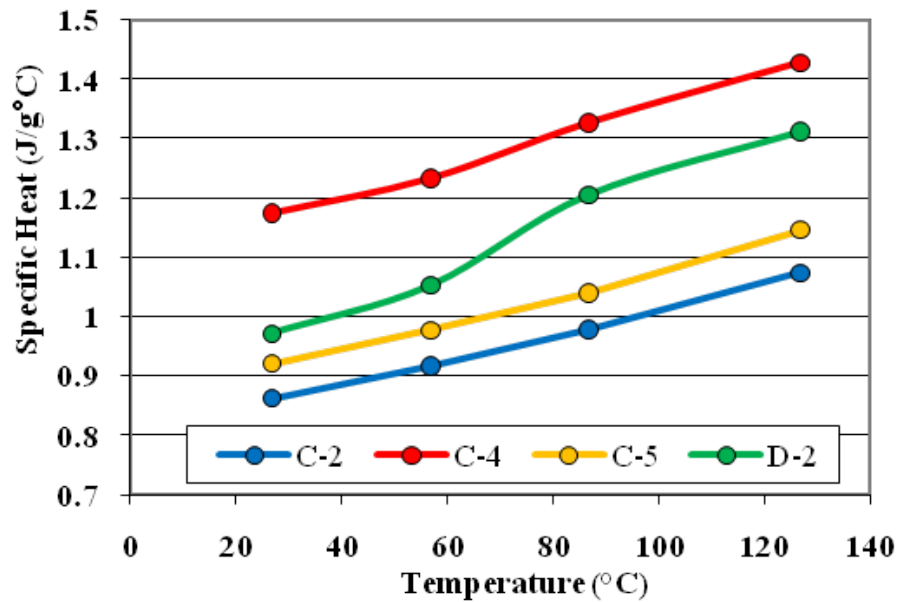


**Figure 4.10:** Typical specific heat values for different locations.

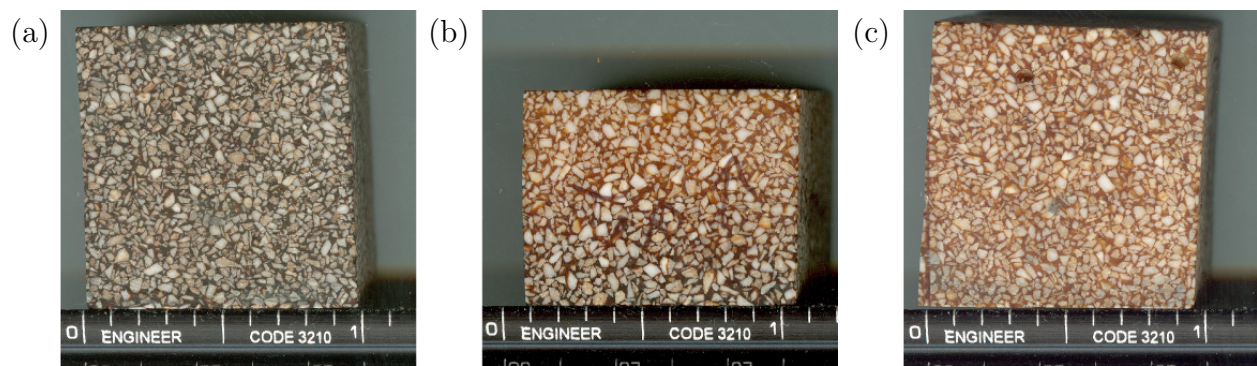


**Figure 4.11:** Images of sample after performing a conductivity test, where (a) is the bottom, (b) is the side, and (c) is the top. (Note: the scale is in inches).

to ensure that any residual chemical reactions were completed prior to re-measuring the thermal conductivity. Portions of the material were placed in a chamber at 125°C and checked periodically for changes. The changes that were observed are illustrated in Figure 4.12. The exterior surfaces that were exposed to the air in the chamber became increasingly darker over time. However, the interior, shown by the cross-sections in the figure, continued to get lighter over time. The difference in the interior and exterior color is illustrated in Figure 4.13, where it can be seen that the darkening of the exterior surface only extends approximately 2 mm deep. The slit, shown in Figure 4.13, was cut prior to placing the material in the chamber, and inspection of the discoloration along its surface shows that the darkening of the exterior occurs wherever the material is exposed to air.

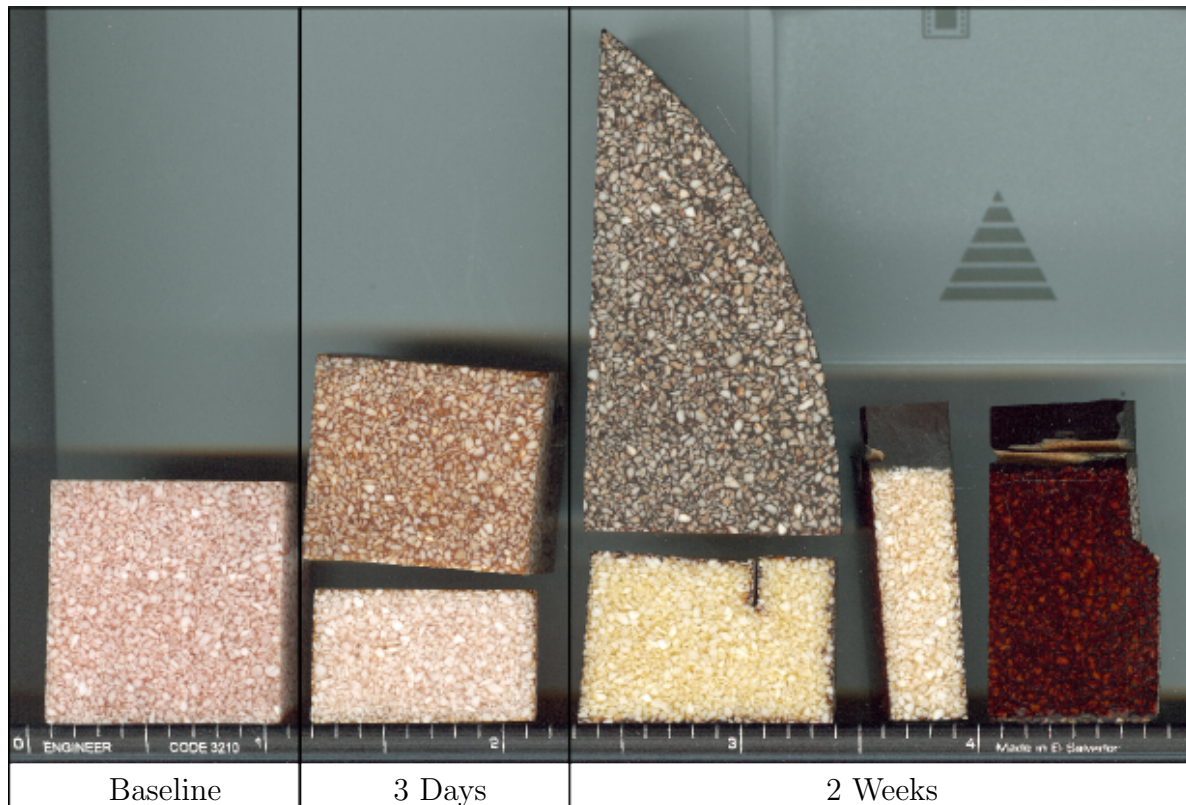


**Figure 4.12:** Changes in the material after being exposed exposed to 125°C for the given time, where at 3 days and 2 weeks the darker surfaces are the exterior color and the lighter surfaces are cross sections to show the interior color.

A section of the material was placed in a chamber at 125°C and monitored for changes in color and changes in mass until it reached a steady state. Three samples, with thickniesses

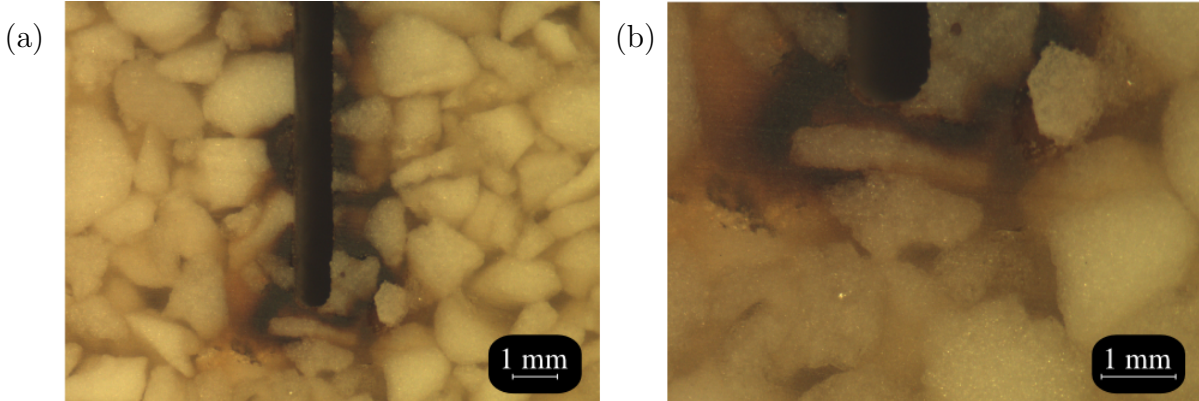


**Figure 4.13:** Micrographs showing the surface effects which occurred after being held at 125°C for 2 weeks.

of 7.3 mm, 15.7 mm, and 19.6 mm were then cut from this section to perform the thermal conductivity tests. They were tested with mean sample temperatures of 25, 75, and 100°C. The apparent thermal conductivities at these temperatures are shown in Table 4.2.

**Table 4.2:** Apparent thermal conductivity values measured at given temperatures.

Temperature (°C)	$\lambda$ (W/m · K)
25	1.96
75	2.85
100	3.17

It should be noted that this method assumes the thermal conductivity to be the same for each sample. However, it is expected that the thermal conductivity will vary with the volume fraction, particle size, and number of particles of alumina. Since the volume fraction was found to vary by location, and therefore by sample, it is not possible to determine the local thermal conductivity of a specific sample. Rather, the values reported represent the average apparent thermal conductivity of the three samples tested.

## Chapter 5

### Conclusion

A non-destructive method was used to monitor the effect of thermal cycling on the thermal conductivity and delamination of two thermal adhesives. By testing on a standardized, application-specific, package, the data obtained can be used to make design decisions with confidence that the results are indicative of real world performance.

It was found that the clamped PSA, unclamped PSA, and the clamped alternative adhesive showed an increase in thermal performance with cycling, possibly due to curing, which supports earlier findings in the literature. There were no signs of delamination in the PSA after 1000 cycles. However, delamination was detected at 17 out of the 35 locations tested in the boards attached with the alternative adhesive.

While the method used is not capable of detecting the presence of delamination in overmolded boards, it was seen that the thermal conductivity of the PSA adhesive showed similar improvements due to curing with the overmolding as it did without the overmolding. It was also found that severe cracking occurred in overmolding A after 250 cycles while no cracking occurred in overmolding B after 1000 cycles.

volume fraction, specific heat, and thermal conductivity of an epoxy impregnated with alumina granules were measured. The properties were found to be non-uniform both spatially and temporally.

The volume fraction of alumina was measured using optical microscopy and image processing. It was found to vary by location, both axially and radially. However, even the lowest volume fractions measured were still higher than the statistically predicted volume fraction for spherical particles [22]. This is attributed to the process used to combine the epoxy and alumina granules and the range of particle sizes in the mixture.

The specific heat was measured with a DSC and was found to vary by location, ranging from 0.86–1.14 J/g · K at 25°C and 1.07–1.37 J/g · K at 125°C. This is consistent with the conclusion of other authors [1, 2, 3, 4] that the thermal properties are strongly dependent on volume fraction.

The apparent thermal conductivity was measured using a guarded heater method based on the ASTM D5470-06 and was found to range from 1.96 W/m · K at 25°C to 3.17 W/m · K at 100°C. Since only three samples were tested, the authors hope to extend this study to a larger, more statistically significant, dataset in the future.

There were changes in thermal properties and coloration with exposure to temperatures above 60°C. This is attributed to the epoxy not being fully cured as delivered by the vendor. Since these temperatures are within the operating range of many electronics, care needs to be taken to ensure that the potting compound is fully cured prior to deployment. Otherwise, the properties of the potting compound could change drastically and non-uniformly over the life of the product, leading to unpredictable behavior.

Epoxy with embedded alumina granules can be used to improve the thermal performance and reliability of electronics in harsh environments. However, users of such compounds should be aware that the thermal properties are not necessarily constant in time or uniform, and assuming that they are could lead to significant errors when modeling their performance.

## Bibliography

- [1] L. M. McGrath, R. S. Parnas, S. H. King, J. L. Schroeder, D. A. Fischer, and J. L. Lenhart, “Investigation of the thermal, mechanical, and fracture properties of alumina-epoxy composites,” *Polymer*, vol. 49, no. 4, pp. 999–1014, 2008.
- [2] C. P. Wong and R. S. Bollamplaly, “Thermal conductivity, elastic modulus, and coefficient of thermal expansion of polymer composites filled with ceramic particles for electronic packaging,” *Journal of Applied Polymer Science*, vol. 74, no. 14, pp. 3396–3403, 1999.
- [3] Y. P. Mamunya, V. V. Davydenko, P. Pissis, and E. V. Lebdev, “Electrical and thermal conductivity of polymers filled with metal powders,” *European Polymer Journal*, vol. 38, no. 9, pp. 1887–1897, 2002.
- [4] V. Singh, A. R. Kulkarni, and T. R. R. Mohan, “Dielectric properties of aluminum-epoxy composites,” *Journal of Applied Polymer Science*, vol. 90, pp. 3602–3608, 2003 2003.
- [5] J. P. Gwinn and R. L. Webb, “Performance and testing of thermal interface materials,” *Microelectronics Journal*, vol. 34, pp. 215–222, 2003.
- [6] W. Nakayama and A. Bergles, “Thermal interfacing techniques for electronic equipment—a perspective,” *Journal of Electronic Packaging*, vol. 125, pp. 192–199, June 2003.
- [7] C. T. Murray, R. L. Rudman, M. B. Sabade, and A. V. Pocius, “Conductive adhesives for electronic assemblies,” *MRS Bulletin*, pp. 449–454, June 2003.
- [8] S. Murray, C. Hillman, and M. Pecht, “Environmental aging and deadhesion of siloxane-polyimide-epoxy adhesive,” *IEEE Transactions on Components and Packaging Technologies*, vol. 26, pp. 524–531, September 2003.
- [9] T. Tuhus and A. Bjorneklett, “Thermal cycling reliability of die bonding adhesives,” in *Proceeding of 31st Annual International Reliability Physics Symposium*, pp. 204–208, March 1993.
- [10] W.-S. Kwon, M.-J. Yim, K.-W. Paik, S.-J. Ham, and S.-B. Lee, “Thermal cycling reliability and delamination of anisotropic conductive adhesives flip chip on organic substrates with emphasis on the thermal deformation,” *Journal of Electronic Packaging*, vol. 127, pp. 86–90, June 2005.

- [11] V. Eveloy, P. Rodgers, and M. Pecht, "Reliability of pressure-sensitive adhesive tapes for heat sink attachment in air-cooled electronic assemblies," *IEEE Transactions on Device and Materials Reliability*, vol. 4, pp. 650–657, December 2004.
- [12] L. M. Eyman and G. B. Kromann, "Investigation of heat sink attach methodologies and the effects on package structural integrity and interconnect reliability of the 119-lead plastic ball grid array," in *Proceedings of 47th Electronic Components and Technology Conference*, pp. 1068–1075, May 1997.
- [13] V. Khuu, M. Osterman, A. Bar-Cohen, and M. Pecht, "Thermal performance measurements of thermal interface materials using the laser flash method," in *Proceedings of IPACK2007*, no. 33554, July 2007.
- [14] C. Creton, "Pressure-sensitive adhesives: An introductory course," *MRS Bulletin*, pp. 434–439, June 2003.
- [15] R. Conner and J. Peterson, "Electrical grade pressure sensitive adhesive tapes," *Electrical Electronics Insulation Conference*, pp. 697–700, September 1995.
- [16] D. Klosterman, L. Li, and J. E. Morris, "Materials characterization, conduction development, and curing effects on reliability of isotropically conductive adhesives," *IEEE Transactions on Components, Packaging, and Manufacturing Technology—Part A*, vol. 21, pp. 23–31, March 1998.
- [17] Q. Yao and J. Qu, "Interfacial versus cohesive failure on polymer-metal interfaces in electronic packaging – effects of interface roughness," *Journal of Electronic Packaging*, vol. 124, pp. 127–134, June 2002.
- [18] C. J. M. Lasance, "The urgent need for widely-accepted test methods for thermal interface materials," *19th IEEE SEMI-THERM Symposium*, pp. 123–128, 2003.
- [19] R. W. Knight, Y. Elkady, J. C. Suhling, and P. Lall, "Causes of degradation of thermal performance of ball grid arrays after thermal cycling," in *Proceedings of IPACK2007*, no. 33626, 2007.
- [20] P. Lall, M. Islam, J. Evans, J. Suhling, and T. Shete, "Damage mechanics of electronics on metal-backed substrates in harsh environments," *IEEE Transactions on Components and Packaging Technologies*, vol. 29, pp. 204–212, March 2006.
- [21] J. L. Evans, P. Lall, R. Knight, E. Crain, T. Shete, and J. R. Thompson, "System design issues for harsh environment electronics employing metal-backed laminate substrates," *IEEE Transactions on Components and Packaging Technologies*, vol. 31, pp. 74–85, March 2008.
- [22] R. K. McGeary, "Mechanical pacing of spherical particles," *Journal of the American Ceramic Society*, vol. 44, no. 10, pp. 513–522, 1961.

- [23] ASTM D5470-06, *Standard Test Method for Thermal Transmission Properties of Thermally Conductive Electrical Insulation Materials*. ASTM International, PA, United States.
- [24] Y. A. Elkady, *Thermal Performance of Ball Grid Arrays and Thin Interface Materials*. PhD thesis, Auburn University, Auburn, AL, United States, 2005.

## Appendices